NOTES AND CORRESPONDENCE

A Summary of North Atlantic Baroclinic Variability

CARL WUNSCH

Department of Earth, Atmospheric, and Planetary Sciences, Massachusetts Institute of Technology, Cambridge, Massachusetts

7 April 1998 and 9 June 1999

ABSTRACT

The modal decomposition, proportional amplitudes, and lateral spatial scale of baroclinic motions in the North Atlantic Ocean are described as determined from more than 20 years of moored instrument data. The subtropical and subpolar gyres emerge naturally as regions of distinct energy levels, in the ratio of potential to kinetic energy, and in horizontal wavelength. Data in other ocean basins prove too sparse to use.

1. Introduction

As part of an effort by the author and others to systematically and quantitatively test basin and global-scale oceanic general circulation models (GCMs) against observations, we have compiled a number of basic observations of oceanic baroclinic variability. As GCMs become more realistic, the data required to quantitatively test them on more than a small regional scale become scarce. An ultimate goal, not undertaken here, is the production of a general spectral description of low-frequency oceanic variability. The interim results are summarized now in the hope that they will be of use to others engaged in similar enterprises.

Another, related, motivation arises from preparations for assimilating temperature and salinity profiles from profiling floats (PALACE floats: R. Davis and B. Owens 1997, personal communication) into a general circulation model. One requires estimates of the variance expected owing to mesoscale variability. If the model is not eddy-resolving, that variance becomes a measure of the extent to which the model must be permitted to deviate from the observations. If the model is eddy-resolving and if it had the skill to reproduce the eddies in detail, the variance becomes an a priori estimate of the solution variance.

Here we use the quasi-global current meter mooring compilation used by Wunsch (1997, 1999) to discuss the vertical modal partition of the baroclinic variability. Many, but not all, current meter records are accompanied by temperature records and it is these observations that are employed. The main goal is to map as far as practical with the limited available coverage, the rms movement of the main thermocline and the vertical mode partition. As important by-products, we obtain a modal decomposition which can be compared to that for the velocity field in Wunsch (1997, hereafter W97), and through the ratio of the estimated kinetic/potential energies for the low modes, an estimate of the spatial scale as a function of position, of the mesoscale variability.

In principle, all results are functions of frequency, wavenumber, and geographical position. Here geography is emphasized and the frequency/wavenumber properties are integrated out—although we will make an estimate of the dominant wavelength. In the frequency domain (e.g., W97 or Wunsch 1999), the records tend to be dominated by motions near 100 days, and it is in that sense we are dealing with the lumped mesoscale variability.

2. Potential energy and length scales

Some notation is required, but the details are omitted; see, for example, Wunsch and Stammer (1997) or Moore and Philander (1977) for what is a standard derivation. With the conventional definitions of u, v, w, p, assume the separation of variables

$$(u, v) = [U(x, y, t), V(x, y, t)]F(z) \quad (1)$$

$$w = P(x, y, t)G(z) \quad (2)$$

$$p = \rho_0 P(x, y, t)F(z). \quad (3)$$

From the equations of motion, one has, for a fixed frequency σ,

Corresponding author address: Dr. Carl Wunsch, Department of Earth, Atmospheric, and Planetary Sciences, Rm. 54-1520, Massachusetts Institute of Technology, Cambridge, MA 02139-4307.
E-mail: cwunsch@pond.mit.edu

$$\overline{G}_n(z) \equiv \frac{G_n(z)}{-i\sigma} = -\frac{1}{N(z)^2}\frac{dF_n(z)}{dz}, \tag{4}$$

and

$$\frac{G_n'(z)}{-i\sigma} = \gamma_n^2 F_n(z), \qquad n = 0, 1, 2, \cdots, \tag{5}$$

$$\frac{d^2G_n(z)}{dz^2} + N^2(z)\gamma_n^2 G_n(z) = 0, \tag{6}$$

$$\frac{d}{dz}\left(\frac{1}{N(z)^2}\frac{dF_n}{dz}\right) + \gamma_n^2 F_n(z) = 0; \tag{7}$$

$N(z)$ is the buoyancy frequency. Both (6) and (7) are subject to boundary conditions at $z = 0, -h$, where the latter is the water depth. These equations define a discrete set of vertical modes, whose shape, $F_n(z)$, $G_n(z)$, and eigenvalues, γ_n^2, are independent of frequency, and with corresponding horizontal structures, $P_n(x, y, t)$, etc.

A vertical normalization is required. For consistency with Wunsch (1997), we take

$$\int_{-h}^{0} F_n(z)^2\, dz = 1. \tag{8}$$

It follows that

$$\int_{-h}^{0} \frac{1}{N^2}\left(\frac{dF_n(z)}{dz}\right)^2 dz = \int_{-h}^{0} N^2(z)\overline{G}_n(z)^2\, dz = \gamma_n^2 \int_{-h}^{0} F_n^2(z)\, dz = \gamma_n^2. \tag{9}$$

The "equivalent depth" is $h_n = 1/(g\gamma_n^2)$. For consistency of units, if $F_n(z)$ is dimensionless, then $[U] = \mathrm{L/T}$, $[G] = \mathrm{T/L}$, $[P] = \mathrm{L^2/T^2}$, $[\gamma_n^2] = \mathrm{T^2/L^2}$.

a. Potential energy

The potential energy is

$$\mathrm{PE} = \frac{1}{2}\int_{-h}^{0} N^2(z)\eta^2(z)\, dz. \tag{10}$$

Here η is the vertical displacement of an isotherm or isopycnal. The vertical normal mode representation is from (2),

$$\eta(x, y, z, t) = \sum_{n=1}^{M} P_n(x, y, t)\overline{G}_n(z), \tag{11}$$

where M is a cutoff mode number in what is necessarily a finite sum. The barotropic mode, $n = 0$, is omitted. $P_n(x, y, t)$ are computed by fitting Eq. (11) in the vertical to

$$\eta(x, y, z_j, t) = -\frac{\theta'(x, y, z_j, t)}{\partial\overline{\theta}/\partial z}, \tag{12}$$

where $\overline{\theta}$ is the mean vertical temperature profile, and θ' is the local temperature minus its time mean. The empirically estimated coefficients are called

$$\tilde{\alpha}_n(x, y, t) \equiv P_n(x, y, t), \tag{13}$$

with the tilde denoting an estimate of the true value α_n. The potential energy estimate is then

$$\mathrm{PE} = \sum_{n=1}^{M} \overline{P_n(x, y, t)^2}\int_{-h}^{0} \frac{N^2(z)}{2}\overline{G}_n(z)^2\, dz = \frac{1}{2}\sum_{n=1}^{M} \overline{\tilde{\alpha}_n(t)^2}\gamma_n^2, \tag{14}$$

where the overbar denotes the time average. The last expression depends upon

$$\int_{-h}^{0} N^2(z)\overline{G}_q(z)\overline{G}_n(z)\, dz = \gamma_q^2\delta_{qn}, \tag{15}$$

which requires the rigid-lid approximation, $\overline{G}_n(0) = 0$.

b. Length scales

The ratio of kinetic to potential energy is

$$\mathcal{R} = \frac{\displaystyle\int_{-h}^{0} (u^2 + v^2)\, dz}{\displaystyle\int_{-h}^{0} (1/N^2)(\partial p/\partial z)^2\, dz}. \tag{16}$$

In the geostrophic limit, assume there is a dominant wavenumber, (k, l). Then, for mode, n,

$$\mathcal{R}_n = \frac{(k^2 + l^2)\displaystyle\int_{-h}^{0} F_n^2(z)\, dz}{f^2\displaystyle\int_{-h}^{0} 1/N^2(z)(dF_n/dz)^2\, dz} = \frac{(k^2 + l^2)\displaystyle\int_{-h}^{0} F_n^2(z)\, dz}{f^2\displaystyle\int_{-h}^{0} N^2(z)\overline{G}_n^2\, dz} = \frac{k^2 + l^2}{f^2\gamma_n^2} = \frac{(k^2 + l^2)gh_n}{f^2} = (k^2 + l^2)R_n^2 \tag{17}$$

where R_n is the Rossby radius of the nth mode. Suppose $R_{nD} = 50$ km (any mode) and the wavelength $\lambda = 500$ km. Then $\mathcal{R}_n \approx 0.4$.

Equation (17) permits one to solve for the dominant wavelength:

$$\lambda_n = 2\pi R_n/\sqrt{\mathcal{R}_n} = 2\pi/(\sqrt{\mathcal{R}_n}f\gamma_n), \tag{18}$$

producing an estimate of the spatial scales in the mesoscale variability, which is otherwise difficult to obtain from in situ observations.

3. Data and analysis

Several results of the numerical fitting of the 105 moorings are of interest. First, however, it must be said that determination of the vertical displacement modes

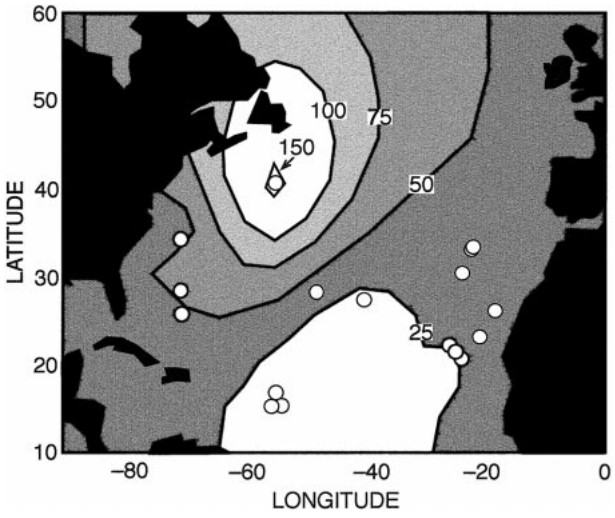

FIG. 1a. Rms vertical displacements in meters from instruments lying in the range of 1–300-m depth.

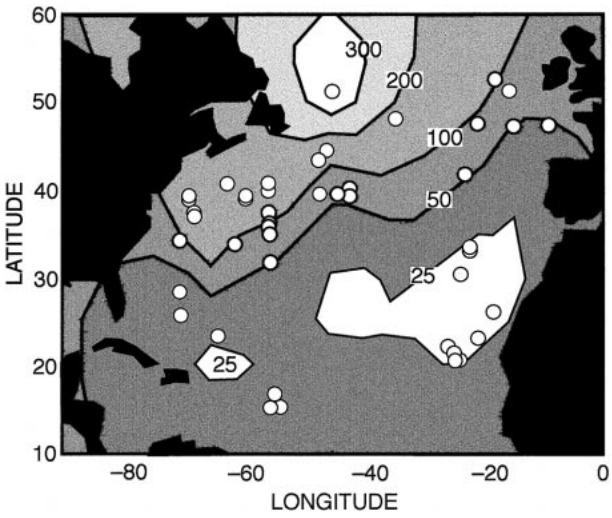

FIG. 1b. Same as Fig. 1a except for the depth range of 300–900 m, straddling the main thermocline. Outlier near 50°N, 312°E appears to be real.

is more difficult than for the velocity modes discussed in W97. A number of current meters failed to produce a useful temperature record over all or part of the data duration (although pure temperature recorders do exist, all instruments here were combined velocity/temperature measuring devices; we will refer to them simply as ''current meters''). Many instruments were set very close to the bottom of the abyssal ocean where the temperature signal is extremely weak (unlike the velocity field) and many such records are dominated by their least-count noise.

The mean vertical temperature profiles, $\partial\overline{\theta}/\partial z$, were obtained from the Levitus and Boyer (1994) climatology. In a significant number of locations their deepest estimated value of temperature lay well above the position of the deepest instrument. A few profiles were extrapolated, but in view of the weak signals, the instrument was often simply dropped from the calculation. In many cases, the number of useful records on any particular mooring was smaller than the already small number of current records. Consequently, the number of modes being fit was reduced from the five used in W97 for currents (including the barotropic mode) to three for temperature (not including the barotropic mode).

The a priori variance for the estimates was set as

$$[\langle\alpha_1^2\rangle, \langle\alpha_2^2\rangle, \langle\alpha_3^2\rangle] \propto [1, 1/2, 1/4]. \qquad (19)$$

These a priori values influence the results only when the number of usable instruments on a mooring is less than three (see Wunsch 1996). Because the modal potential energy is proportional to $\gamma_i^2\alpha_i^2$ rather than α_i^2, the prior statistics differ from assuming that modal energy is in the ratio in Eq. (19). For a variety of reasons, including the availability of only two records, or because of extremely poor fits—in equatorial regions—the results from 13 moorings were suppressed. A fixed a priori estimate of rms temperature measurement error of 0.1°C was used (see W97). Better values could be obtained through an instrument-by-instrument analysis, but such an effort would probably not qualitatively change our results.

Results are sensitive to the values of $\partial\overline{\theta}/\partial z$ and the reliability of the climatological values is not at all clear, particularly as in many regions there are very few abyssal measurements. Furthermore, in the energetic regions of the ocean, any particular one-year temperature record may have been obtained in a significantly different regime from the long-term average. Thus, as with the results in W97 but further exaggerated here, the results should be regarded as only semiquantitative. Nonetheless, as in W97, to the extent that large-scale patterns emerge from the extremely inhomogeneous records, one can have some confidence in the results. In the end however, the discussion here is confined to the North Atlantic; formal errors for the estimated $\tilde{\alpha}_i$ from the many three-instrument North Pacific moorings render the results there too uncertain for a clear discussion.

4. North Atlantic results

Figure 1a depicts the estimated rms vertical displacement obtained from instruments (not modal fits) in the depth range from 0 to 300 m. Figure 1b shows the values in the range 300–900 m, chosen to straddle the main thermocline. The subtropical gyre essentially corresponds to the region where the vertical displacements are 50 m or less. These displacements grow to order 200 m in the Gulf Stream system. In the main thermocline, a single mooring near 51°N, 315°E shows as an isolated extreme point. Results from this mooring are anomalous in a number of ways in their extreme values, and it perhaps should have been omitted; there

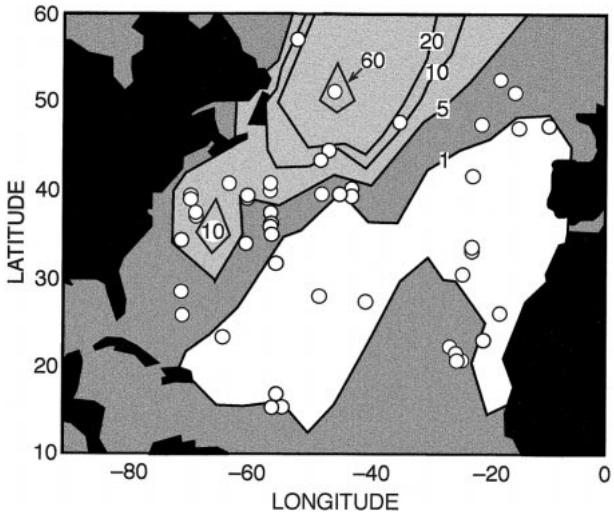

FIG. 1c. Estimated potential energy/unit mass (in $m^2\ s^{-2} \times 100$) from the first three baroclinic modes integrated in the vertical.

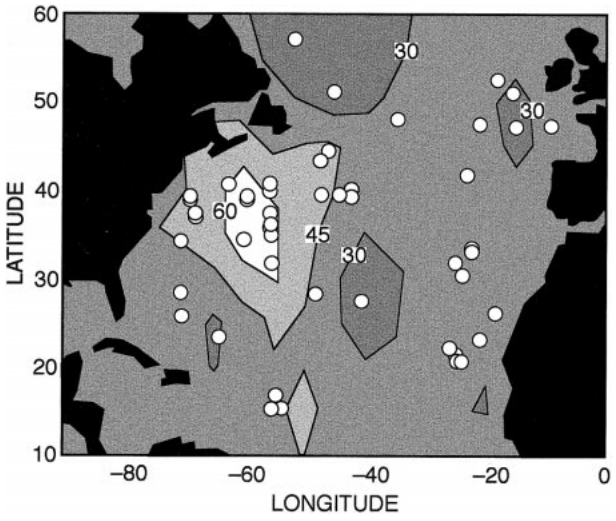

FIG. 1d. Percentage of the potential energy in Fig. 1c lying in the first baroclinic mode. The high percentage southeast of Nova Scotia may be associated with the seamount chains in this area.

is otherwise no reason, however, to reject it. The reader is reminded (see W97, Fig. 19), that many moorings in and near the Gulf Stream system undergo large vertical displacements, thus producing biased results when assigned to a fixed depth.

The estimated vertically integrated total potential energy/unit mass is displayed in Fig. 1c. Most of the subtropical gyre has values near 100 $m^2\ s^{-2}$, rising into the Gulf Stream system to about 10 times the water column average kinetic energy. (Note that in W97, the corresponding plots for kinetic energy density were of the *logarithm* of the value.) The pattern is roughly similar to Dantzler's (1977) estimate of potential energy density based upon the vertical displacement of the 15° isotherm as seen in bathythermograph data.

Moorings near 15°N, 50°–55°W fail to show the energy increase visible in Dantzler's map and in the altimetric variability maps (the latter are discussed in Wunsch 1999). This region is one of expected baroclinic instability (Gill et al. 1974). The moored data in question were discussed by Fu et al. (1982), who concluded that there was no evidence for such instability. But the inconsistency of the mooring data with an ever-growing set of other observations now strongly suggests that the one year of data available to Fu et al. was simply unrepresentative of the average conditions in this region. A multiyear revisit with moorings to this area would be very useful.

Figure 1d displays the fraction of the water-column-average potential energy in Fig. 1c that is contained in the first baroclinic mode. On average, the value is 30%–40% of the total, being highest, over 50%, near the Gulf Stream southeast of Nova Scotia and near the seamount chains.

The ratio $\mathcal{R}_1$ of estimated kinetic energy in mode 1 to the estimated potential energy in that mode is shown in Fig. 2a. As is generally expected for mesoscale variability, the potential energy is dominant everywhere, being proportionally largest in the region of high kinetic energy associated with the Gulf Stream, and with the kinetic energy proportionally largest in the interior subtropical gyre at about 27°N. The potential energy outlier near 51°N, 45°W, has disappeared in the ratio.

Böning and Budich (1992, Table 2) estimated the ratio of total eddy kinetic energy to total eddy potential energy in the subtropical gyre as about $1/2.1^2 \approx 0.23$ in a numerical model with horizontal resolution of $0.33° \times 0.4°$ (meridional by zonal); this value apparently contained the contribution from mode-0 kinetic energy, the barotropic energy. To produce a comparable statistic, Fig. 2b shows the ratio of the kinetic energy in modes 0–3 to the potential energy in modes 1–3. As a visual

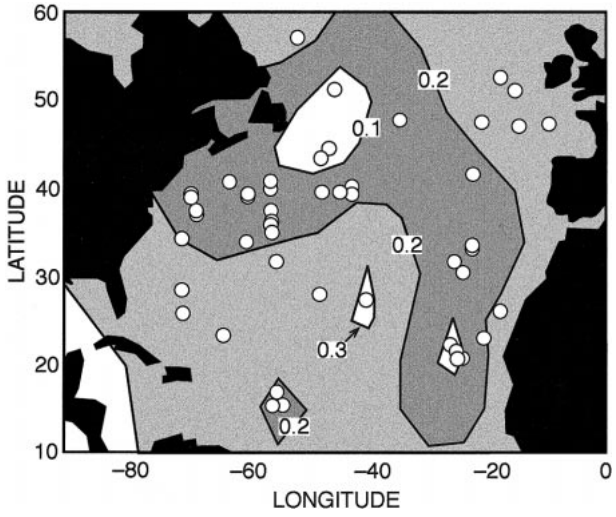

FIG. 2a. Ratio of kinetic to potential energies in the first baroclinic mode [see Eq. (17)].

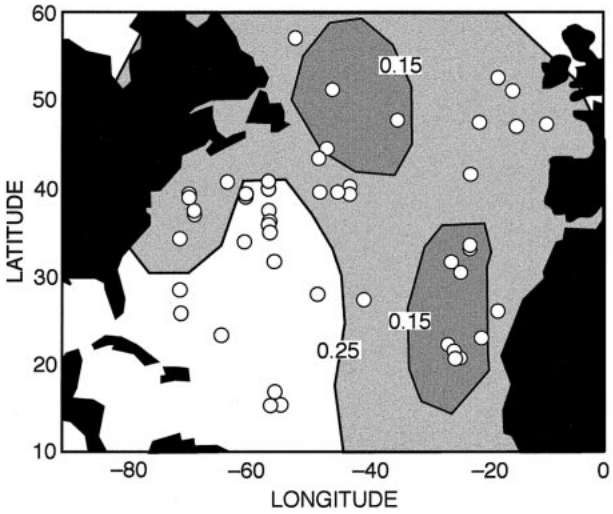

FIG. 2b. Same as Fig. 2a except for the total kinetic (including the barotropic mode) energy in the eddy field.

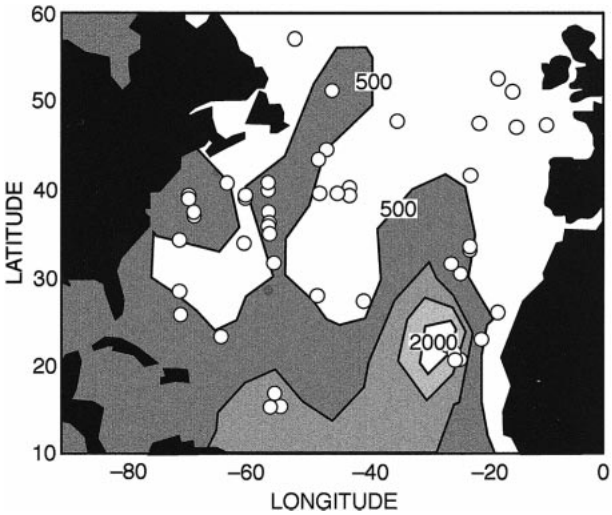

FIG. 3. Estimate of λ_1, the horizontal wavelength of the motions in the first baroclinic mode (in km).

spatial average, the Böning and Budich (1992) value is quite a good one. Their estimated value for the subpolar gyre was about $1/2.3^2 = 0.18$, which is again crudely consistent with what we observe. Thus their particular model appears to be generating eddy energy ratios, which are roughly correct.

Perhaps more interesting is the calculation of the wavelength λ_1 from Eq. (18) shown in Fig. 3. In general terms, one sees the expected growth toward low latitudes, reflecting the increase there in the Rossby radius of deformation. The Gulf Stream/North Atlantic Current region appears to carry a somewhat longer wavelength disturbance into high latitudes. Most previous estimates of spatial scale of the variability have been based upon spatial-lag correlation functions (e.g., Stammer and Böning 1996; Stammer 1997). The relationship between their scale, L_0, defined as the first zero-crossing of the spatially lagged autocorrelation, and their L_1 obtained from the correlation integral, and λ_1 is not very clear, as a decorrelation scale will depend upon wavenumber content and anisotropy in a way that is different from the factors determining λ_1. If one defines ''scale'' as $l_1 = \lambda_1/4$, then the mooring-implied scale is bracketed in this latitude range as $L_1 \leq l_1 \leq L_0$ (their Fig. 6.11). The general decline seen in l_1 with latitude follows L_0 as corrected by Stammer (1997), whereas L_1 is nearly constant with latitude.

At any given location, there exists a frequency/wavenumber spectrum of variability. The employment of λ_1 reduces the wavenumber spectrum to a single moment—a clear oversimplification of the actual situation—but one having the advantage of greatly reducing the number of descriptive parameters, be it in the observations or in model results. There is a connection between the spatial scale obtained here and the theories of baroclinic and barotropic instability, as well as providing a useful model test. The reader is referred to Stammer and Böning (1996) and Stammer (1998) for a discussion.

Other oceans

Spatial coverage by moorings in the North Pacific is very limited (see the chart in W97) and, as already noted, the vertical distribution of instruments is quite thin. North Pacific results are thus much more sensitive than those in the North Atlantic to the a priori assumptions [Eq. (19)]; the results have very large formal error estimates, and are therefore not shown here.

Moored data also exist in the South Atlantic, Indian, and Southern Oceans, including a number of moorings with more than three instruments in the vertical. All were analyzed, but the lateral coverage is even sparser than in the North Pacific, rendering any spatial patterns wholly dependent upon the accidents of coverage. We therefore refrain from any further discussion except to note the complete failure of the low-mode hypothesis on the equatorial moorings.

Acknowledgments. Supported in part by NASA Grant NAG5-3724. Contribution to the World Ocean Circulation Experiment.

REFERENCES

Böning, C. W., and R. G. Budich, 1992: Eddy dynamics in a primitive equation model: Sensitivity to horizontal resolution and friction. *J. Phys. Oceanogr.*, **22,** 361–381.

Dantzler, H. L., Jr., 1977: Potential energy maxima in the tropical and subtropical North Atlantic. *J. Phys. Oceanogr.*, **7,** 512–519.

Fu, L.-l., T. Keffer, P. Niiler, and C. Wunsch, 1982: Observations of mesoscale variability in the western North Atlantic: A comparative study. *J. Mar. Res.*, **40,** 809–848.

Gill, A. E., J. S. A. Green, and A. J. Simmons, 1974: Energy partition in the large-scale ocean circulation and the production of mid-ocean eddies. *Deep-Sea Res.*, **21,** 499–528.

Levitus, S. and T. P. Boyer, 1994: *World Ocean Atlas 1994*. U.S. Govt. Printing Office, 117 pp.

Moore, D. W., and S. G. H. Philander, 1977: Modeling of the tropical oceanic circulation. *The Sea. Vol. 6: Ideas and Observations on Progress in the Study of the Seas,* E. D. Goldberg, I. N. McCave, J. J. O'Brien, and J. H. Steele, Eds., Wiley-Interscience, 319–361.

Stammer, D., 1997: Global characteristics of ocean variability from regional TOPEX/Posedion altimeter measurements. *J. Phys. Oceanogr.*, **27,** 1743–1769.

——, 1998: On eddy characteristics, eddy mixing and mean flow properties. *J. Phys. Oceanogr.*, **28,** 727–739.

——, and C. Böning, 1996: Generation and distribution of mesoscale eddies in the North Atlantic Ocean. *Warm Water Sphere of the North Atlantic Ocean,* W. Krauss, Ed., Gebrüder Bornträger, 159–163.

Wunsch, C., 1996: *The Ocean Circulation Inverse Problem.* Cambridge University Press, 437 pp.

——, 1997: The vertical partition of horizontal kinetic energy and the spectrum of global variability. *J. Phys. Oceanogr.*, **27,** 1770–1794.

——, 1999: Where do ocean eddy heat fluxes matter? *J. Geophys. Res.,* **104,** 13 235–13 250.

——, and D. Stammer, 1997: Atmospheric loading and the ''inverted barometer'' effect. *Rev. Geophys.,* **35,** 79–107.